



Yan Qing Wang · Hu Long Zhao

# Free vibration analysis of metal foam core sandwich beams on elastic foundation using Chebyshev collocation method

Received: 6 March 2019 / Accepted: 27 June 2019 / Published online: 6 July 2019  
© Springer-Verlag GmbH Germany, part of Springer Nature 2019

**Abstract** In this paper, free vibration of a metal foam core sandwich (MFCS) beam embedded in Winkler–Pasternak elastic foundation is studied using the Chebyshev collocation method (CCM). This method can achieve high precision within the range allowed by the effective number of bits of computers. Three foam distribution types along the thickness direction are considered for the core. The Timoshenko beam theory is adopted and Hamilton’s principle is utilized to derive the boundary conditions and governing equations of the model. The numerical results show that natural frequencies of the sandwich beam initially increase and then decrease with the rise in thickness of metal foam core. By arranging the foam distribution in the core, natural frequencies of the sandwich beam can be significantly changed. Moreover, natural frequencies of the uniform foam distribution beam are insensitive to the foam coefficient. For the beam with non-uniform foam distribution, however, the natural frequencies increase or decrease with the foam coefficient, depending closely on the foam type. In addition, the present method is validated by comparing with the published ones for special cases.

**Keywords** Metal foam core sandwich beam · Chebyshev collocation method · Free vibration · Timoshenko beam theory · Winkler–Pasternak foundation

## 1 Introduction

Metal foam, as a novel class of porous materials, has a series of advantages such as good thermal insulation, low density, excellent capacity of damping and effective capacity of energy dissipation [1]. One can disperse foams continuously and smoothly along one or more directions to adjust the local parameter of metal foams for achieving specific functions. Due to their excellent characteristics, metal foam structures have attracted much attention and their mechanical properties have been studied by some researchers. Chen et al. [2] utilized the Timoshenko beam theory to analyze forced and free vibrations of metal foam beams. Jabbari et al. [3] explored the buckling problem of metal foam beams using the classical plate theory. Rezaei and Saidi [4] studied free vibration of beams made of metal foams based on the Carrera unified formulation. By utilizing the Timoshenko and Euler–Bernoulli beam theories, Wang et al. [5] performed wave propagation analysis of a metal foam beam. Jasion et al. [6] presented global and local buckling analysis of metal foam plates utilizing the finite element method. Zheng et al. [7] used a cell-based finite element model to analyze dynamic uniaxial

Y. Q. Wang (✉) · H. L. Zhao  
Department of Mechanics, Northeastern University, Shenyang 110819, China  
E-mail: wangyanqing@mail.neu.edu.cn

Y. Q. Wang  
Key Laboratory of Ministry of Education on Safe Mining of Deep Metal Mines, Northeastern University, Shenyang 110819, China

impact behavior of metal foams. Liu et al. [8] investigated the dynamic behavior of metal foam material via the impact Hopkinson bar test. Wang et al. [9] studied the nonlinear vibration of a cylindrical shell made of metal foam materials.

Structural mechanical behaviors have attracted much attention of researchers [10–26]. Sandwich structures have a wide range of applications in aerospace, transportation and civil engineering industries. Typically, sandwich structure consists of three parts: two single face layers and a core [27–30]. Metal foam as the core of sandwich structures has many advantages such as high energy absorption ability, high resistance to impact, high strength-to-weight ratio and high stiffness-to-weight ratio [31–33]. Thus, some researches have paid their attention to this type of structures. Zhang et al. [34] studied the low-velocity impact response of MFCS beams using numerical, experimental and analytical methods. Jing et al. [35] analyzed the failure and deformation modes of MFCS beams via experiment. By utilizing the finite element method, the mechanical impedance of MFCS beams was investigated by Streck et al. [36]. Grygorowicz et al. [37] presented buckling analysis of MFCS beams by using the ANSYS software. Under the three-point bending testing, Omar et al. [38] investigated the flexural properties of MFCS beams. Smyczynski and Magnucka-Blandzi [39] explored the stability problem of sandwich beams with metal foam core. Caliskan and Apalak [40] experimentally investigated low-velocity impact bending response of MFCS beams.

Usually, structures are embedded in elastic foundations in engineering applications. Winkler's elastic foundation [41], a widely used one-parameter model [42–47], is consisted of countless closed-spaced linear springs. Winkler's foundation assumes no interaction between the springs, and the continuity of the foundation soil is not considered. In order to avoid this limitation, several two-parameter models were proposed [48–53]. Among them, the Winkler–Pasternak elastic foundation considers the interaction among the points in the foundation and the effect of transverse shear deformation of the foundation. Therefore, the Winkler–Pasternak elastic foundation is a more accurate model to depict the elastic foundation effect on structures [54–61].

The Chebyshev collocation method is a kind of numerical methods based on the Chebyshev polynomials of the first kind. It is worth mentioning that this method can achieve high precision within the range allowed by the effective number of bits of computers. This method can solve ordinary differential equations and its main advantage is that it is easy to deal with the singularity problem. In particular, the Chebyshev collocation method possesses a better computational accuracy and efficiency than Galerkin's method and finite element method [62,63].

In the existing literature, vibration of MFCS beams embedded in Winkler–Pasternak elastic foundation has not been investigated. In this article, the CCM is applied to investigate free vibration of this advanced structure. The Timoshenko beam theory is used to model the present system. Three types of foam distribution for the core are considered. Hamilton's principle is used to obtain boundary conditions and governing equations. Additionally, the influences of various parameters are discussed on the free vibration of MFCS beams.

## 2 Theory and formulation

### 2.1 Metal foam core sandwich beam

A sandwich beam with metal foam core embedded in the Winkler–Pasternak elastic foundation is shown in Fig. 1. The top and bottom face layers of the beam are steel, and the core is steel foam. It is assumed that the face layers are bonded perfectly to the core. The width and length of the beam are denoted by  $b$  and  $L$ , respectively. The total thickness of the sandwich beam  $h_t$  is  $h_t = h_c + 2h_1$ , where  $h_c$  and  $h_1$  are the thicknesses of the core and single face layer, respectively. The Winkler parameter and Pasternak parameter of the Winkler–Pasternak elastic foundation are  $K_w$  and  $K_p$ , respectively. For the core, three types of foam distribution are considered, as shown in Fig. 2.

The largest size pore is located at the mid-plane of core for non-uniform foam distribution 1 (foam-I) while at the bottom and top surfaces of the core for non-uniform foam distribution 2 (foam-II). For the uniform foam distribution (foam-III), the pore size is constant. The material properties of metal foam core are expressed by using Eqs. (1)–(3) [64–66].

foam-I:

$$\begin{cases} E(z) = E_1 \left[ 1 - \vartheta_0 \cos\left(\frac{\pi z}{h_c}\right) \right] \\ \rho(z) = \rho_1 \left[ 1 - \vartheta_m \cos\left(\frac{\pi z}{h_c}\right) \right] \end{cases} \quad (1)$$

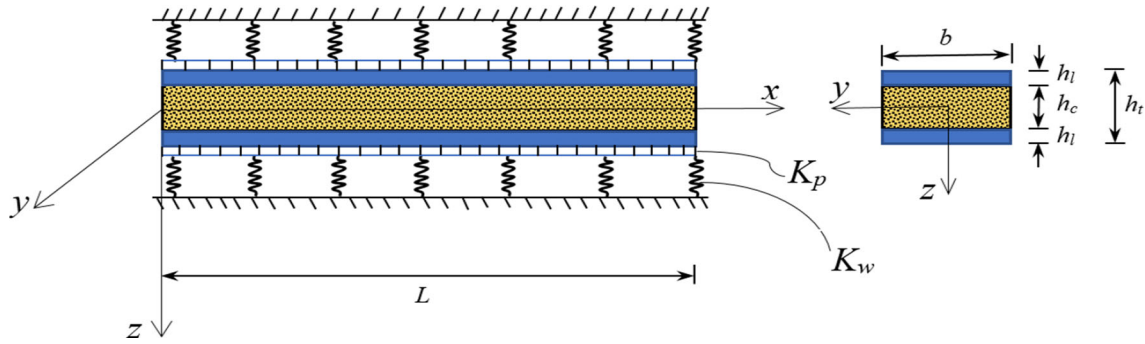


Fig. 1 Metal foam core sandwich beam

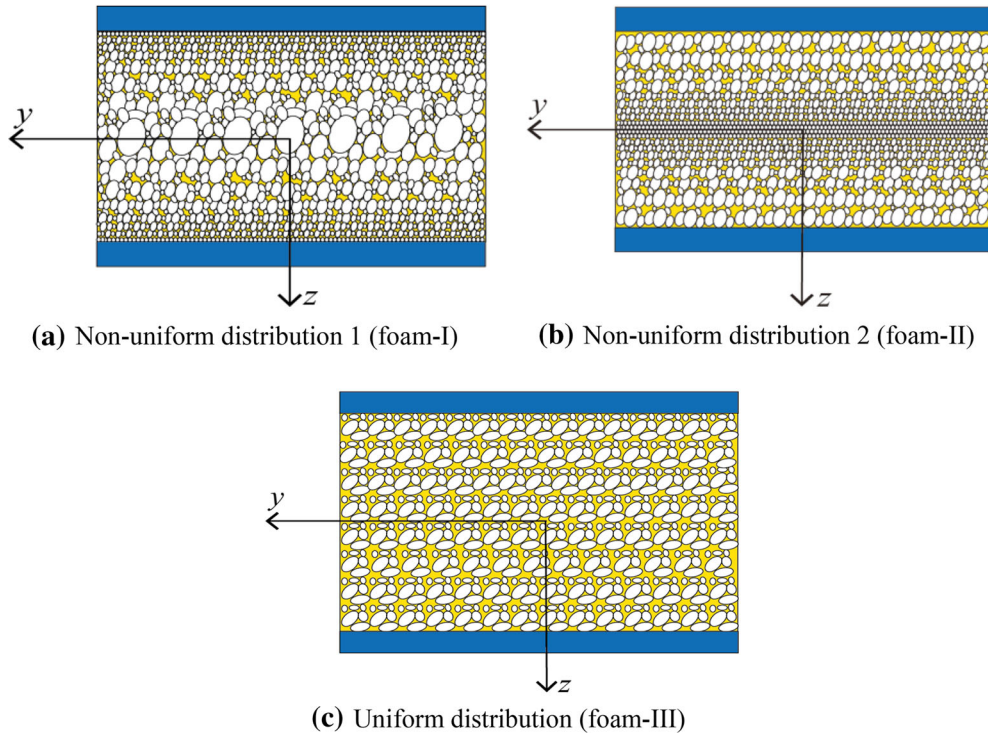


Fig. 2 Beam cross section

foam-II:

$$\begin{cases} E(z) = E_1 \left\{ 1 - \vartheta_0^* \left[ 1 - \cos \left( \frac{\pi z}{h_c} \right) \right] \right\} \\ \rho(z) = \rho_1 \left\{ 1 - \vartheta_m^* \left[ 1 - \cos \left( \frac{\pi z}{h_c} \right) \right] \right\} \end{cases} \quad (2)$$

foam-III:

$$\begin{cases} E = E_1 \varphi \\ \rho = \rho_1 \varphi^* \end{cases} \quad (3)$$

where  $E(z)$  and  $\rho(z)$  are Young's modulus and mass density of the metal foam core, respectively;  $E_1$  and  $\rho_1$  are the maximum values of Young's modulus and mass density of the metal foam core, respectively, which are equal to those values of pure steel;  $\vartheta_0$ ,  $\vartheta_0^*$  and  $\varphi$  are foam coefficients for foam-I, foam-II and foam-III, respectively;  $\vartheta_m$ ,  $\vartheta_m^*$  and  $\varphi^*$  are corresponding coefficients of mass density.

For open-cell metal foams, we have [64,67,68]

$$\frac{E(z)}{E_1} = \left( \frac{\rho(z)}{\rho_1} \right)^2. \quad (4)$$

**Table 1** Foam coefficients for different foam distributions

$\vartheta_0$	$\vartheta_0^*$	$\varphi$
0.1	0.1738	0.9361
0.2	0.3442	0.8716
0.3	0.5103	0.8064
0.4	0.6708	0.7404
0.5	0.8231	0.6733
0.6	0.9612	0.6047

The relationships between foam coefficients and mass density coefficients are expressed as

$$\begin{cases} 1 - \vartheta_m \cos\left(\frac{\pi z}{h_c}\right) = \sqrt{1 - \vartheta_0 \cos\left(\frac{\pi z}{h_c}\right)} & \text{foam-I} \\ 1 - \vartheta_m^* \left[1 - \cos\left(\frac{\pi z}{h_c}\right)\right] = \sqrt{1 - \vartheta_0^* \left[1 - \cos\left(\frac{\pi z}{h_c}\right)\right]} & \text{foam-II} \\ \varphi^* = \sqrt{\varphi} & \text{foam-III} \end{cases} \quad (5)$$

Without the loss of generality, the masses of beams with different metal foam core are considered to be equal to each other, so we have

$$\int_0^{h_c/2} \sqrt{1 - \vartheta_0 \cos\left(\frac{\pi z}{h_c}\right)} dz = \int_0^{h_c/2} \sqrt{1 - \vartheta_0^* \left[1 - \cos\left(\frac{\pi z}{h_c}\right)\right]} dz = \int_0^{h_c/2} \sqrt{\varphi} dz. \quad (6)$$

which is utilized to determine  $\vartheta_0^*$  and  $\varphi$  with a given value of  $\vartheta_0$ . These values are shown in Table 1. It is noted that  $\vartheta_0^*$  increases with  $\vartheta_0$  and is close to the upper limit (0.9612) when  $\vartheta_0 = 0.6$ . Hence, in the following numerical calculations,  $\vartheta_0 \in [0, 0.6]$  is adopted.

### 2.2 Governing equations

According to the Timoshenko beam theory, the displacement components of an arbitrary point in the beam can be described by [69]

$$\begin{cases} u_x(x, z, t) = u(x, t) + z\psi(x, t) \\ u_y(x, z, t) = 0 \\ u_z(x, z, t) = w(x, t) \end{cases} \quad (7)$$

in which  $u_x$ ,  $u_y$  and  $u_z$  are  $x$ -,  $y$ - and  $z$ - components of the displacement vector, respectively;  $u$  and  $w$  are axial and transverse displacements of a point on the mid-plane of the beam, respectively;  $\psi$  is rotation of the cross section of the beam; and  $t$  is time.

From Eq. (7), the normal strain  $\varepsilon_{xx}$  and shear strain  $\gamma_{xz}$  are obtained as

$$\varepsilon_{xx} = z \frac{\partial \psi}{\partial x} + \frac{\partial u}{\partial x}, \quad \gamma_{xz} = \psi + \frac{\partial w}{\partial x}. \quad (8)$$

The normal stress  $\sigma_{xx}$  and shear stress  $\tau_{xz}$  are expressed as [70]

$$\sigma_{xx} = E\varepsilon_{xx}, \quad \tau_{xz} = \frac{E}{2(1 + \nu)}\gamma_{xz} \quad (9)$$

where  $\nu$  is Poisson’s ratio. It is assumed that metal foam core has the same Poisson’s ratio as steel.

The first variation of the strain energy  $U_s$  is written as

$$\begin{aligned} \delta U_s &= \int_0^L \int_A (\sigma_{xx} \delta \varepsilon_{xx} + \tau_{xz} \delta \gamma_{xz}) dA dx \\ &= \int_0^L \left[ N_x \left( \delta \frac{\partial u}{\partial x} \right) + M_x \left( \delta \frac{\partial \psi}{\partial x} \right) + Q_x \left( \delta \frac{\partial w}{\partial x} + \delta \psi \right) \right] dx \end{aligned} \quad (10)$$

where  $A$  is the area of cross section of the beam;  $N_x$  is the axial force,  $M_x$  is the bending moment and  $Q_x$  is the transverse shear force. These stress resultants are defined by

$$N_x = A_{11} \frac{\partial u}{\partial x} + B_{11} \frac{\partial \psi}{\partial x}, \quad M_x = B_{11} \frac{\partial u}{\partial x} + D_{11} \frac{\partial \psi}{\partial x}, \quad Q_x = K_s A_{55} \left( \frac{\partial w}{\partial x} + \psi \right) \quad (11)$$

in which  $K_s = 5/6$  is the shear correction factor and

$$\begin{aligned} A_{11} &= \int_{h_c/2}^{h_t/2} E_1 b dz + \int_{-h_c/2}^{h_c/2} E(z) b dz + \int_{-h_t/2}^{-h_c/2} E_1 b dz \\ B_{11} &= \int_{h_c/2}^{h_t/2} E_1 b z dz + \int_{-h_c/2}^{h_c/2} E(z) b z dz + \int_{-h_t/2}^{-h_c/2} E_1 b z dz \\ D_{11} &= \int_{h_c/2}^{h_t/2} E_1 b z^2 dz + \int_{-h_c/2}^{h_c/2} E(z) b z^2 dz + \int_{-h_t/2}^{-h_c/2} E_1 b z^2 dz \\ A_{55} &= \frac{1}{2(1+\nu)} \left( \int_{h_c/2}^{h_t/2} E_1 b dz + \int_{-h_c/2}^{h_c/2} E(z) b dz + \int_{-h_t/2}^{-h_c/2} E_1 b dz \right). \end{aligned} \quad (12)$$

The first variation of additional strain energy from the elastic foundation is expressed as [55]

$$\delta U_{ad} = \int_0^L \left( K_w w \delta w + K_p \frac{\partial w}{\partial x} \frac{\partial \delta w}{\partial x} \right) dx. \quad (13)$$

The kinetic energy of the beam can be written as

$$K = \int_0^L \int_A \frac{1}{2} \rho \left[ \left( \frac{\partial u_x}{\partial t} \right)^2 + \left( \frac{\partial u_y}{\partial t} \right)^2 + \left( \frac{\partial u_z}{\partial t} \right)^2 \right] dA dx. \quad (14)$$

The first variation of the kinetic energy is given by

$$\delta K = \int_0^L \left[ I_0 \left( \frac{\partial u}{\partial t} \frac{\partial \delta u}{\partial t} + \frac{\partial w}{\partial t} \frac{\partial \delta w}{\partial t} \right) + I_1 \left( \frac{\partial \psi}{\partial t} \frac{\partial \delta u}{\partial t} + \frac{\partial u}{\partial t} \frac{\partial \delta \psi}{\partial t} \right) + I_2 \frac{\partial \psi}{\partial t} \frac{\partial \delta \psi}{\partial t} \right] dx \quad (15)$$

where

$$\begin{aligned} I_0 &= \int_{h_c/2}^{h_t/2} \rho_1 b dz + \int_{-h_c/2}^{h_c/2} \rho(z) b dz + \int_{-h_t/2}^{-h_c/2} \rho_1 b dz \\ I_1 &= \int_{h_c/2}^{h_t/2} \rho_1 b z dz + \int_{-h_c/2}^{h_c/2} \rho(z) b z dz + \int_{-h_t/2}^{-h_c/2} \rho_1 b z dz \\ I_2 &= \int_{h_c/2}^{h_t/2} \rho_1 b z^2 dz + \int_{-h_c/2}^{h_c/2} \rho(z) b z^2 dz + \int_{-h_t/2}^{-h_c/2} \rho_1 b z^2 dz. \end{aligned}$$

Based on Hamilton's principle, one obtains [71]

$$\int_{t_1}^{t_2} \delta (U_s + U_{ad} - K) dt = 0. \quad (16)$$

Applying Eqs. (10), (13) and (15) in Eq. (16), the following governing equations are obtained:

$$\begin{cases} \frac{\partial N_x}{\partial x} = I_0 \frac{\partial^2 u}{\partial t^2} + I_1 \frac{\partial^2 \psi}{\partial t^2} \\ \frac{\partial Q_x}{\partial x} - K_w w + K_p \frac{\partial^2 w}{\partial x^2} = I_0 \frac{\partial^2 w}{\partial t^2} \\ \frac{\partial M_x}{\partial x} - Q_x = I_2 \frac{\partial^2 \psi}{\partial t^2} + I_1 \frac{\partial^2 u}{\partial t^2} \end{cases} \quad (17)$$

Let us introduce the following dimensionless quantities:

$$\begin{aligned}
 X &= \frac{x}{L}, \quad \eta = \frac{L}{h_t}, \quad \{\bar{U}, \bar{W}\} = \frac{\{u, w\}}{h_t}, \quad A_{00} = E_1 A, \quad I_{00} = \rho_1 A \\
 \{a_{11}, a_{55}, b_{11}, d_{11}\} &= \left\{ \frac{A_{11}}{A_{00}}, \frac{A_{55}}{A_{00}}, \frac{B_{11}}{A_{00}h_t}, \frac{D_{11}}{A_{00}h_t^2} \right\}, \quad \{\bar{I}_0, \bar{I}_1, \bar{I}_2\} = \left\{ \frac{I_0}{I_{00}}, \frac{I_1}{I_{00}h_t}, \frac{I_2}{I_{00}h_t^2} \right\} \\
 \bar{K}_w &= \frac{K_w L^4}{A_{00}h_t^2}, \quad \bar{K}_p = \frac{K_p L^2}{A_{00}h_t^2}, \quad \tau = \frac{t}{L} \sqrt{\frac{A_{00}}{I_{00}}}, \quad \omega_n = \Omega_n L \sqrt{\frac{I_{00}}{A_{00}}}
 \end{aligned} \tag{18}$$

in which  $\Omega_n$  and  $\omega_n$  ( $n = 1, 2, 3 \dots$ ) are dimensional and non-dimensional natural frequencies, respectively.

By using Eq. (18) in Eq. (17), the dimensionless governing equations are stated as

$$\begin{cases}
 a_{11} \frac{\partial^2 \bar{U}}{\partial X^2} + b_{11} \frac{\partial^2 \psi}{\partial X^2} = \bar{I}_0 \frac{\partial^2 \bar{U}}{\partial \tau^2} + \bar{I}_1 \frac{\partial^2 \psi}{\partial \tau^2} \\
 \eta^2 K_s a_{55} \left( \frac{\partial^2 \bar{W}}{\partial X^2} + \eta \frac{\partial \psi}{\partial X} \right) - \bar{K}_w \bar{W} + \bar{K}_p \frac{\partial^2 \bar{W}}{\partial X^2} = \eta^2 \bar{I}_0 \frac{\partial^2 \bar{W}}{\partial \tau^2} \\
 b_{11} \frac{\partial^2 \bar{U}}{\partial X^2} + d_{11} \frac{\partial^2 \psi}{\partial X^2} - K_s a_{55} \eta \left( \frac{\partial \bar{W}}{\partial X} + \eta \psi \right) = \left( \bar{I}_1 \frac{\partial^2 \bar{U}}{\partial \tau^2} + \bar{I}_2 \frac{\partial^2 \psi}{\partial \tau^2} \right)
 \end{cases} \tag{19}$$

and the dimensionless boundary conditions are written as

Clamped (C):

$$\bar{W} = \bar{U} = \psi = 0. \tag{20}$$

Hinged (H):

$$\bar{W} = \bar{U} = b_{11} \frac{\partial \bar{U}}{\partial X} + d_{11} \frac{\partial \psi}{\partial X} = 0. \tag{21}$$

### 3 Chebyshev collocation method

In the Chebyshev collocation method (CCM), the Chebyshev interpolation grid points in the interval  $[-1, 1]$  are constructed by using Gauss–Chebyshev–Lobatto collocation grid points, which are written as [72]

$$x_j = \cos \left( \frac{j\pi}{N} \right), \quad j = 0, 1, 2, 3, \dots, N. \tag{22}$$

Then, the  $(N + 1) \times (N + 1)$  Chebyshev differentiation matrix  $\mathbf{D}_1$  can be constructed by using the Chebyshev collocation points. Herein, Lagrange polynomials of degree  $N$  are interpolated at each Chebyshev point. Differentiating the polynomials, and then evaluating the result at the collocation points, all elements in the matrix are obtained as

$$\begin{aligned}
 (D_1)_{00} &= \frac{2N^2+1}{6}, \quad (D_1)_{NN} = -\frac{2N^2+1}{6} \\
 (D_1)_{jj} &= -\frac{x_j}{2(1-x_j^2)}, \quad j = 1, 2, 3, \dots, N-1 \\
 (D_1)_{ij} &= \frac{c_i(-1)^{i+j}}{c_j(x_i-x_j)}, \quad i \neq j, i, j = 0, 1, 2, \dots, N
 \end{aligned} \tag{23}$$

where

$$c_i = \begin{cases} 2, & i = 0 \text{ or } N \\ 1, & \text{otherwise} \end{cases}. \tag{24}$$

The second-order differentiation matrix is defined as  $\mathbf{D}_2 = (\mathbf{D}_1)^2$  and so on for the higher-order differentiation matrices.

### 4 Application of CCM

In order to apply the CCM, firstly, we change the range of the independent variables in Eqs. (19)–(21) from  $X \in [0, 1]$  to  $\xi = (2X - 1) \in [-1, 1]$ .

The displacement functions of the sandwich beam for harmonic vibration are written as:

$$\begin{cases} \bar{U}(X, \tau) = U(X)e^{i\omega_n\tau} \\ \bar{W}(X, \tau) = W(X)e^{i\omega_n\tau} \\ \psi(X, \tau) = \phi(X)e^{i\omega_n\tau} \end{cases} \quad (25)$$

in which  $i = \sqrt{-1}$ . By applying Eq. (25) in Eqs. (19)–(21) and using the range of the independent variables  $\xi$ , the governing equations are written as

$$\begin{cases} 4a_{11} \frac{\partial^2 U}{\partial \xi^2} + 4b_{11} \frac{\partial^2 \phi}{\partial \xi^2} = -(\bar{I}_0 \omega_n^2 U + \bar{I}_1 \omega_n^2 \phi) \\ \eta^2 K_s a_{55} \left( 4 \frac{\partial^2 W}{\partial \xi^2} + 2\eta \frac{\partial \phi}{\partial \xi} \right) - \bar{K}_w W + 4\bar{K}_p \frac{\partial^2 W}{\partial \xi^2} = -\bar{I}_0 \eta^2 \omega_n^2 W \\ 4b_{11} \frac{\partial^2 U}{\partial \xi^2} + 4d_{11} \frac{\partial^2 \phi}{\partial \xi^2} - K_s a_{55} \eta \left( 2 \frac{\partial W}{\partial \xi} + \eta \phi \right) = -(\bar{I}_1 \omega_n^2 U + \bar{I}_2 \omega_n^2 \phi) \end{cases} \quad (26)$$

and the boundary conditions are stated as

Clamped (C):

$$W = U = \phi = 0. \quad (27)$$

Hinged (H):

$$W = U = 2b_{11} \frac{\partial U}{\partial \xi} + 2d_{11} \frac{\partial \phi}{\partial \xi} = 0. \quad (28)$$

Then, based on the Chebyshev differentiation matrix, the left-hand sides of Eq. (26) are expressed as

$$\begin{aligned} \mathbf{EM1} &= 4b_{11}([0 \ 0 \ 1] \otimes \mathbf{D}_2) + 4a_{11}([1 \ 0 \ 0] \otimes \mathbf{D}_2) \\ \mathbf{EM2} &= \eta^2 K_s a_{55} [4([0 \ 1 \ 0] \otimes \mathbf{D}_2) + 2\eta([0 \ 0 \ 1] \otimes \mathbf{D}_1)] \\ &\quad - \bar{K}_w([0 \ 1 \ 0] \otimes \mathbf{I}_1) + 4\bar{K}_p([0 \ 1 \ 0] \otimes \mathbf{D}_2) \\ \mathbf{EM3} &= 4d_{11}([0 \ 0 \ 1] \otimes \mathbf{D}_2) + 4b_{11}([1 \ 0 \ 0] \otimes \mathbf{D}_2) \\ &\quad - K_s a_{55} \eta [\eta([0 \ 0 \ 1] \otimes \mathbf{I}_1) + 2([0 \ 1 \ 0] \otimes \mathbf{D}_1)] \end{aligned} \quad (29)$$

in which  $\otimes$  is the Kronecker product;  $\mathbf{I}_1$  is identity matrix of size  $(N + 1) \times (N + 1)$ ; and  $\mathbf{D}_2 = (\mathbf{D}_1)^2$  is the second-order differentiation matrix. The size of **EM1**, **EM2** and **EM3** is  $(N + 1) \times 3(N + 1)$ , where  $N$  is the number of Chebyshev points. By stacking these matrices together, the global matrix **EM** of size  $3(N + 1) \times 3(N + 1)$  is achieved:

$$\mathbf{EM} \cdot \delta = \begin{bmatrix} \mathbf{EM1} \\ \mathbf{EM2} \\ \mathbf{EM3} \end{bmatrix} \cdot \delta \quad (30)$$

where  $\delta$  represents the transpose displacement vector in the form of

$$\delta = [U_1 \ U_2 \ \dots \ U_{N+1} \ W_1 \ W_2 \ \dots \ W_{N+1} \ \phi_1 \ \phi_2 \ \dots \ \phi_{N+1}]^T. \quad (31)$$

Therefore, Eq. (26) can be expressed as

$$\begin{bmatrix} \mathbf{EM1} \\ \mathbf{EM2} \\ \mathbf{EM3} \end{bmatrix} \cdot \delta = -\omega_n^2 \begin{bmatrix} \bar{I}_0 \mathbf{I}_1 & \mathbf{0} & \bar{I}_1 \mathbf{I}_1 \\ \mathbf{0} & \bar{I}_0 \eta^2 \mathbf{I}_1 & \mathbf{0} \\ \bar{I}_1 \mathbf{I}_1 & \mathbf{0} & \bar{I}_2 \mathbf{I}_1 \end{bmatrix} \cdot \delta. \quad (32)$$

Based on the CCM, the boundary conditions of the beam at both ends are listed in Table 2.

The displacements of the beam at the left end are defined as  $U_1$ ,  $W_1$  and  $\phi_1$ , and those at the right end are  $U_{N+1}$ ,  $W_{N+1}$  and  $\phi_{N+1}$ . Hence, the displacement vector in Eq. (31) is reworded as

$$\bar{\delta} = [U_1 \ W_1 \ \phi_1 \ U_{N+1} \ W_{N+1} \ \phi_{N+1} \ U_2 \ U_3 \ \dots \ U_N \ W_2 \ W_3 \ \dots \ W_N \ \phi_2 \ \phi_3 \ \dots \ \phi_N]^T. \quad (33)$$



**Table 2** Boundary condition (B.C.) matrices

B.C.	Left edge	Right edge
C–C	$([1\ 0\ 0] \otimes [1\ 0\ \dots\ 0]) \cdot \delta = 0$ $([0\ 1\ 0] \otimes [1\ 0\ \dots\ 0]) \cdot \delta = 0$ $([0\ 0\ 1] \otimes [1\ 0\ \dots\ 0]) \cdot \delta = 0$	$([1\ 0\ 0] \otimes [0\ 0\ \dots\ 1]) \cdot \delta = 0$ $([0\ 1\ 0] \otimes [0\ 0\ \dots\ 1]) \cdot \delta = 0$ $([0\ 0\ 1] \otimes [0\ 0\ \dots\ 1]) \cdot \delta = 0$
C–H	$([1\ 0\ 0] \otimes [1\ 0\ \dots\ 0]) \cdot \delta = 0$ $([0\ 1\ 0] \otimes [1\ 0\ \dots\ 0]) \cdot \delta = 0$ $([0\ 0\ 1] \otimes [1\ 0\ \dots\ 0]) \cdot \delta = 0$	$([1\ 0\ 0] \otimes [0\ 0\ \dots\ 1]) \cdot \delta = 0$ $([0\ 1\ 0] \otimes [0\ 0\ \dots\ 1]) \cdot \delta = 0$ $2d_{11}([0\ 0\ 1] \otimes [D_1(N+1, :)]) \cdot \delta$ $+2b_{11}([1\ 0\ 0] \otimes [D_1(N+1, :)]) \cdot \delta = 0$
H–H	$([1\ 0\ 0] \otimes [1\ 0\ \dots\ 0]) \cdot \delta = 0$ $([0\ 1\ 0] \otimes [1\ 0\ \dots\ 0]) \cdot \delta = 0$ $2b_{11}([1\ 0\ 0] \otimes [D_1(1, :)]) \cdot \delta$ $+2d_{11}([0\ 0\ 1] \otimes [D_1(1, :)]) \cdot \delta = 0$	$([1\ 0\ 0] \otimes [0\ 0\ \dots\ 1]) \cdot \delta = 0$ $([0\ 1\ 0] \otimes [0\ 0\ \dots\ 1]) \cdot \delta = 0$ $2d_{11}([0\ 0\ 1] \otimes [D_1(N+1, :)]) \cdot \delta$ $+2b_{11}([1\ 0\ 0] \otimes [D_1(N+1, :)]) \cdot \delta = 0$

**Table 3** Comparison of dimensionless fundamental natural frequencies of FGM beam under different boundary conditions ( $L/h_t = 10$ )

B.C.	Source	$n = 0$	$n = 0.5$	$n = 1$	$n = 2$	$n = 5$
C–C	Ref. [73]	1.1664	0.9992	0.9056	0.8255	0.7782
	Present	1.1664	0.9992	0.9056	0.8255	0.7782
C–H	Ref. [73]	0.8248	0.7082	0.6456	0.5931	0.5599
	Present	0.8248	0.7082	0.6456	0.5931	0.5599
H–H	Ref. [73]	0.5394	0.4733	0.4449	0.4215	0.3952
	Present	0.5394	0.4733	0.4449	0.4215	0.3952

$n$ : power-law index

By introducing Eq. (33) in Eq. (32), the algebraic system takes the form of

$$\begin{bmatrix} \mathbf{S}_{bb} & \mathbf{S}_{bg} \\ \mathbf{S}_{gb} & \mathbf{S}_{gg} \end{bmatrix} \begin{Bmatrix} \bar{\delta}_b \\ \bar{\delta}_g \end{Bmatrix} = \omega_n^2 \begin{bmatrix} \mathbf{0} & \mathbf{0} \\ \mathbf{0} & \mathbf{M}_{gg} \end{bmatrix} \begin{Bmatrix} \bar{\delta}_b \\ \bar{\delta}_g \end{Bmatrix} \tag{34}$$

where the subscripts “g” and “b” refer to the points used for writing the collocation analog of governing equations and boundary conditions, respectively.  $\mathbf{S}_{bb}$  is a matrix of size  $6 \times 6$ ;  $\mathbf{S}_{bg}$  is a matrix of size  $6 \times [3(N+1)-6]$ ;  $\mathbf{S}_{gb}$  is a matrix of size  $[3(N+1)-6] \times 6$ ; and  $\mathbf{S}_{gg}$  is a matrix of size  $[3(N+1)-6] \times [3(N+1)-6]$ .  $\mathbf{M}_{gg}$  is the dimensionless inertia matrix related to the right-hand side of Eq. (32), and has the same size as  $\mathbf{S}_{gg}$ . This matrix is written as

$$\mathbf{M}_{gg} = - \begin{bmatrix} \bar{I}_0 \mathbf{I} & \mathbf{0} & \bar{I}_1 \mathbf{I} \\ \mathbf{0} & \bar{I}_0 \eta^2 \mathbf{I} & \mathbf{0} \\ \bar{I}_1 \mathbf{I} & \mathbf{0} & \bar{I}_2 \mathbf{I} \end{bmatrix} \tag{35}$$

where  $\mathbf{I}$  is identity matrix of size  $(N-1) \times (N-1)$ . The first component in Eq. (34) is

$$\bar{\delta}_b = -\mathbf{S}_{bb}^{-1} \mathbf{S}_{bg} \bar{\delta}_g \tag{36}$$

and the second component is

$$\mathbf{S}_{gb} \bar{\delta}_b + \mathbf{S}_{gg} \bar{\delta}_g = \omega_n^2 \mathbf{M}_{gg} \bar{\delta}_g \tag{37}$$

From the above formulations, the algebraic eigenvalue equations for free vibration of the MFCS beam are expressed as

$$\left( \mathbf{S}_{gb} \mathbf{S}_{bb}^{-1} \mathbf{S}_{bg} - \mathbf{S}_{gg} + \omega_n^2 \mathbf{M}_{gg} \right) \bar{\delta}_g = \mathbf{0}. \tag{38}$$

### 5 Results and discussion

Due to the inexistence of vibration research of MFCS beams, we consider an FGM beam to validate the present analysis. The material parameters used are as follows: (Aluminum:  $E_m = 70$  GPa,  $\rho_m = 2702$  kg/m<sup>3</sup>,  $\nu_m = 0.3$ ; Alumina:  $E_c = 380$  GPa,  $\rho_c = 3960$  kg/m<sup>3</sup>,  $\nu_c = 0.3$ ). The dimensionless fundamental natural frequencies



**Table 4** Comparison of dimensionless fundamental natural frequencies of metal foam beam under different boundary conditions ( $\vartheta_0 = 0.5$ )

B.C.	$L/h_t$	Porosity distribution 1			Porosity distribution 2		
		Present	Ritz method [2]	ANSYS [2]	Present	Ritz method [2]	ANSYS [2]
H-H	10	0.2798	0.2798	0.2778	0.2599	0.2599	0.2549
	20	0.1422	0.1422	0.1419	0.1318	0.1318	0.1296
	50	0.0571	0.0571	0.0571	0.0529	0.0529	0.0521
C-C	10	0.5947	0.5944	0.6101	0.5476	0.5475	0.5600
	20	0.3167	0.3166	0.3176	0.2888	0.2888	0.2941
	50	0.1291	0.1291	0.1289	0.1174	0.1174	0.1183
C-H	10	0.4243	0.4242	0.4227	0.3899	0.3898	0.3905
	20	0.2203	0.2203	0.2201	0.2013	0.2013	0.2015
	50	0.0891	0.0891	0.0891	0.0813	0.0813	0.0813

**Table 5** Comparison of dimensionless fundamental frequencies of metal foam beam (C-C,  $L/h_t = 20$ )

	$\vartheta_0 = 0$	$\vartheta_0 = 0.2$	$\vartheta_0 = 0.4$	$\vartheta_0 = 0.6$
Ref. [74]	0.3167	0.3144	0.3132	0.3142
Present	0.3173	0.3158	0.3153	0.3168

**Table 6** Convergence of dimensionless fundamental natural frequency  $\omega_1$  of MFCS beam ( $\vartheta_0 = 0.5$ ,  $L = 10h_t$ ,  $K_w = 10^8$ ,  $K_p = 10^6$ ,  $h_c/h_1 = 6$ )

Foam distribution	B.C.	$N = 5$	$N = 6$	$N = 7$	$N = 8$	$N = 9$
foam-I	C-C	0.6508	0.6421	0.6422	0.6423	0.6423
	C-H	0.4719	0.4736	0.4738	0.4737	0.4737
	H-H	0.3363	0.3388	0.3388	0.3387	0.3387
foam-II	C-C	0.6089	0.6002	0.6003	0.6003	0.6003
	C-H	0.4414	0.4430	0.4433	0.4432	0.4432
	H-H	0.3171	0.3194	0.3194	0.3193	0.3193
foam-III	C-C	0.6332	0.6245	0.6246	0.6246	0.6246
	C-H	0.4592	0.4608	0.4611	0.4610	0.4610
	H-H	0.3283	0.3308	0.3307	0.3307	0.3307

**Table 7** The first three dimensionless natural frequencies of MFCS beam ( $\vartheta_0 = 0.5$ ,  $L = 10h_t$ ,  $K_w = 10^8$ ,  $K_p = 10^6$ ,  $h_c/h_1 = 6$ )

Foam distribution	Mode	C-C	C-H	H-H
foam-I	First	0.6423	0.4737	0.3387
	Second	1.5741	1.3405	1.1110
	Third	2.8002	2.5487	2.2896
foam-II	First	0.6003	0.4432	0.3193
	Second	1.4804	1.2532	1.0331
	Third	2.6578	2.4040	2.1462
foam-III	First	0.6246	0.4610	0.3307
	Second	1.5336	1.3034	1.0784
	Third	2.7360	2.4853	2.2286

( $\omega_1 = \Omega_1 L \sqrt{\rho_m/E_m}$ ) from the present analysis are compared with those given by Wattanasakulpong and Chaikittiratana [73], as shown in Table 3. The comparison result depicts very good agreement between them.

To further examine the validity of the present analysis, another two comparison studies are conducted on metal foam beams with different boundary conditions, as shown in Tables 4 and 5. In Table 4, the following material parameters are used: Young's modulus  $E_1 = 200$  GPa, Poisson's ratio  $\nu = 1/3$  and mass density  $\rho_1 = 7850$  kg/m<sup>3</sup>. In Table 5, the following material parameters are used: Young's modulus  $E_1 = 130$  GPa, Poisson's ratio  $\nu = 0.34$  and mass density  $\rho_1 = 8960$  kg/m<sup>3</sup>. The dimensionless natural fundamental frequencies  $\omega_1 = \Omega_1 L \sqrt{\rho_1 (1 - \nu^2)/E_1}$  are calculated and compared with the available results. It can be observed that

**Table 8** The dimensionless fundamental natural frequency  $\omega_1$  of MFCS beam for different foundation parameters ( $\vartheta_0 = 0.5$ ,  $L = 10h_t$ ,  $h_c/h_1 = 6$ )

Foam distribution	B.C.	$(K_w, K_p)$		
		(0, 0)	$(10^8, 0)$	$(10^8, 10^6)$
foam-I	C–C	0.6169	0.6397	0.6423
	C–H	0.4388	0.4703	0.4737
	H–H	0.2885	0.3345	0.3387
foam-II	C–C	0.5730	0.5975	0.6003
	C–H	0.4056	0.4395	0.4432
	H–H	0.2656	0.3149	0.3193
foam-III	C–C	0.5985	0.6219	0.6246
	C–H	0.4250	0.4575	0.4610
	H–H	0.2791	0.3264	0.3307

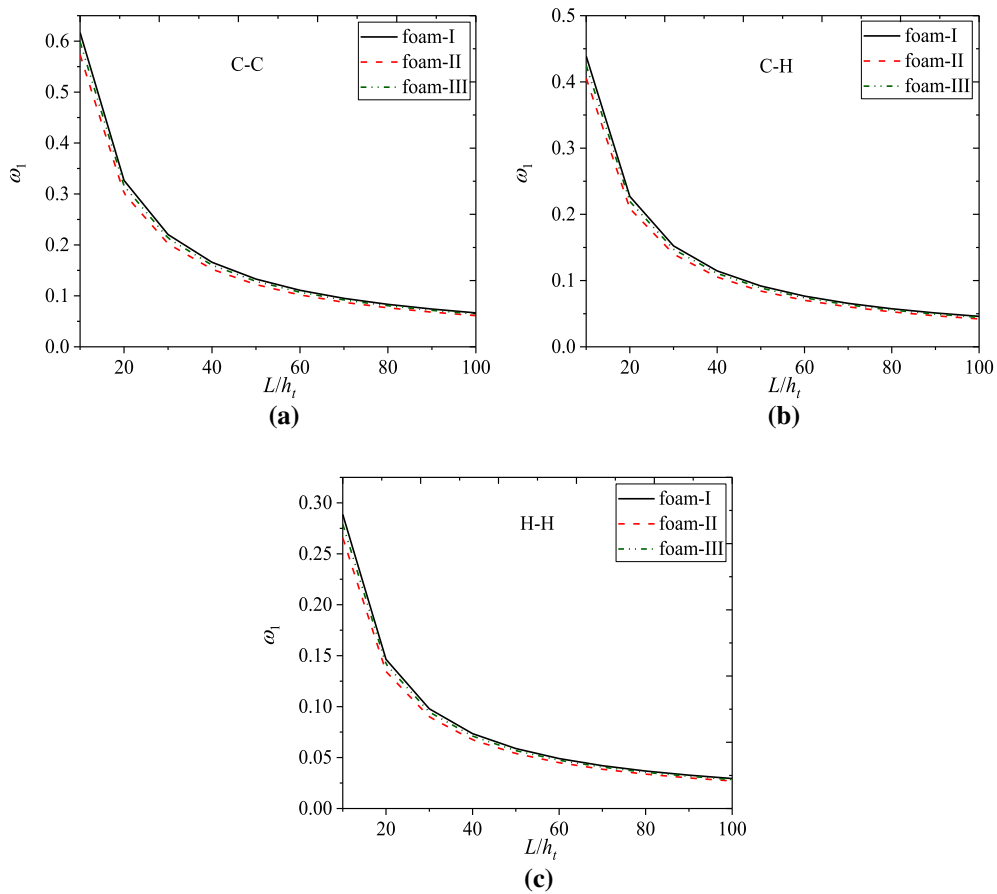
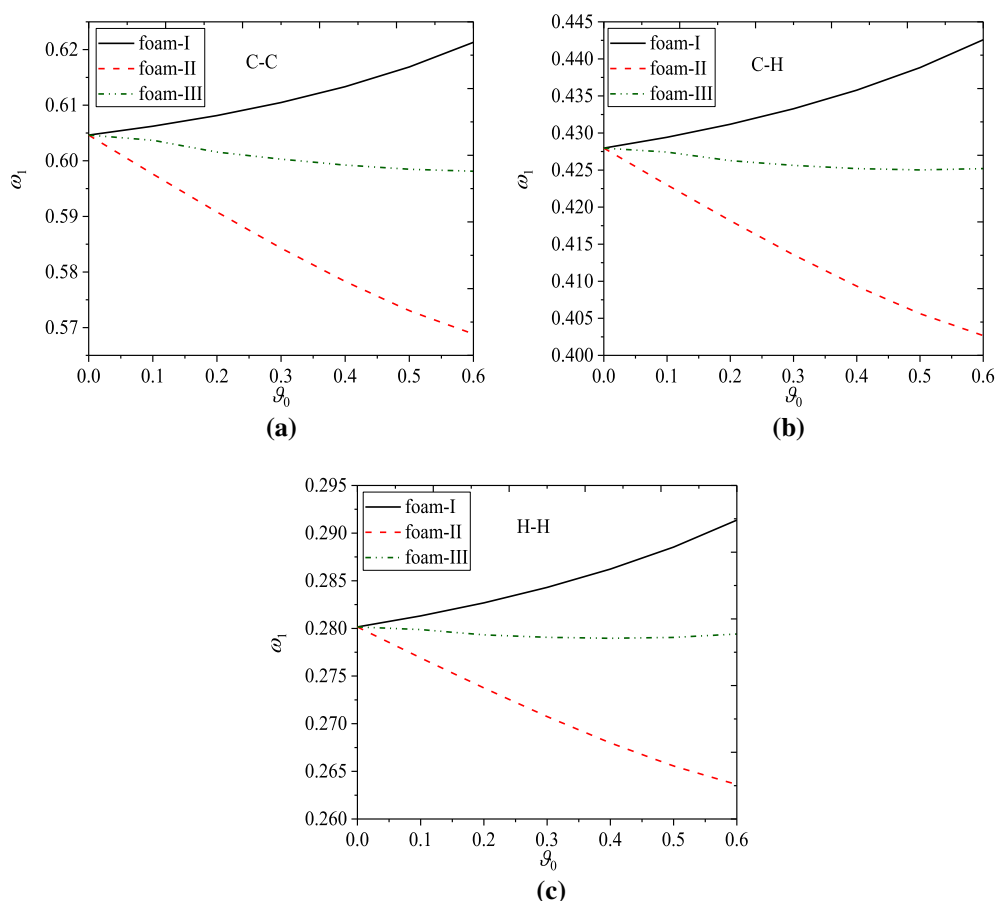


**Fig. 3** Dimensionless fundamental natural frequency versus slenderness ratio ( $k_w = 0$ ,  $k_p = 0$ ,  $\vartheta_0 = 0.5$ ,  $h_c/h_1 = 6$ ): **a** C–C, **b** C–H, **c** H–H

the present results agree well with those given by Chen et al. [2] and Kitipornchai et al. [74], which bespeaks the validity of the present analysis.

In what follows, the MFCS beam shown in Fig. 1 will be dealt with. If not specified, the following geometry and material parameters are used:  $b = 0.2$  m,  $h_t = 0.1$  m,  $E_1 = 200$  GPa,  $\rho_1 = 7850$  kg/m<sup>3</sup>,  $\nu = 0.33$ . The dimensionless natural frequency is introduced as:

$$\omega_n = \Omega_n L \sqrt{\frac{I_{00}}{A_{00}}} \quad (n = 1, 2, 3 \dots).$$



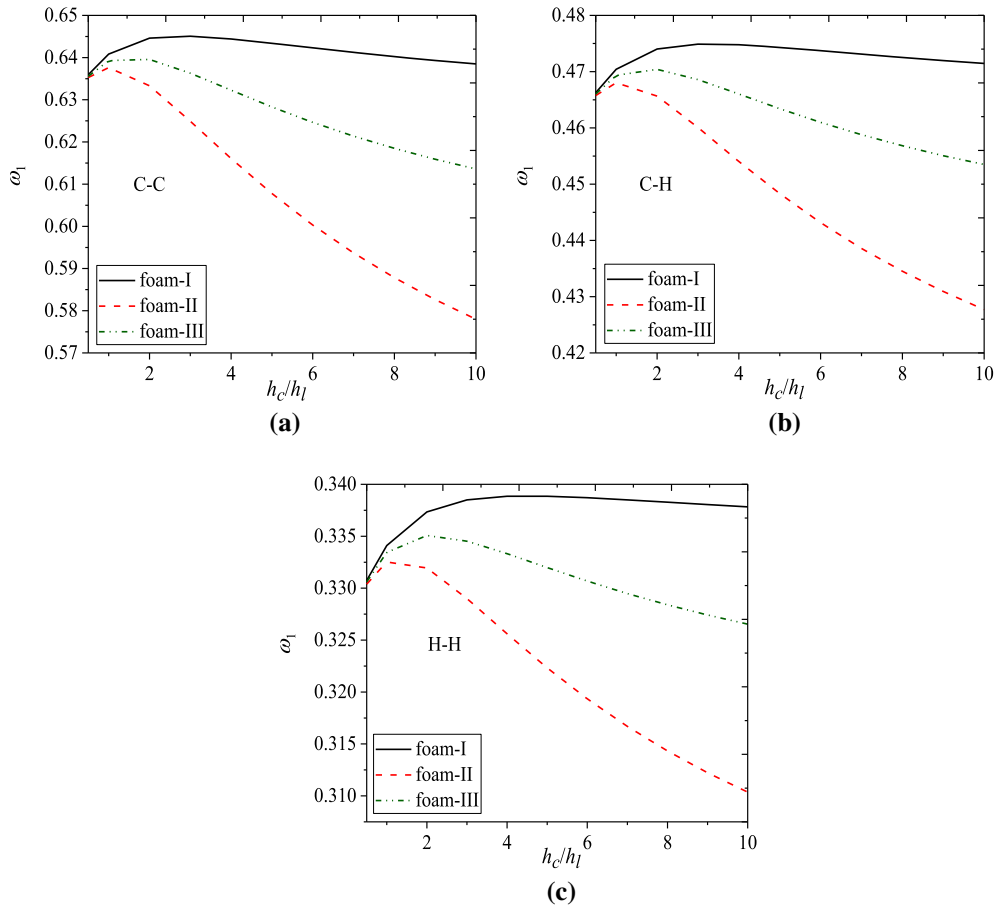
**Fig. 4** Dimensionless fundamental natural frequency versus foam coefficient  $\vartheta_0$  ( $L/h_t = 10$ ,  $k_w = 0$ ,  $k_p = 0$ ,  $h_c/h_1 = 6$ ): **a** C–C, **b** C–H, **c** H–H

Table 6 shows the convergence of dimensionless fundamental natural frequencies of MFCS beams with different boundary conditions and different foam distributions. It is seen that the method has very high rate of convergence; when  $N = 9$ , the natural frequencies for different boundary conditions and different foam distributions converge. Therefore, the number of Chebyshev points, namely,  $N = 9$ , is adopted in the following calculations.

Table 7 illuminates the first three dimensionless natural frequencies of MFCS beams with various foam distributions and boundary conditions. It is noted that the foam-I beam has the highest natural frequency, while the foam-II beam has the lowest natural frequency among different types of foam distribution. This indicates that the foam-I provides the largest structural stiffness, while the foam-II leads to the smallest structural stiffness. In addition, the natural frequency of C–C sandwich beam is the highest while that of H–H sandwich beam is the lowest. This can be expected because C–C edges provide higher level of constraint, while H–H edges provide relatively moderate level of constraint.

Table 8 gives the dimensionless fundamental natural frequencies of the MFCS beam with different foundation parameters. When  $K_w = 0$  and  $K_p = 0$ , it means that the Winkler–Pasternak foundation vanishes. The table shows that when the Winkler foundation exists, the natural frequency of the MFCS beam increases. Moreover, the addition of the Pasternak foundation results in the higher natural frequency of the MFCS beam. This phenomenon shows that the Winkler–Pasternak foundation makes the MFCS beam stiffer.

Figure 3 shows the dimensionless fundamental natural frequency versus slenderness ratio for different boundary conditions and foam distributions. It can be seen that the dimensionless fundamental natural frequency decreases with increasing slenderness ratio. Additionally, when the slenderness ratio is small, the descent rate of natural frequency is rapid. With the further rise in slenderness ratio, the natural frequency changes less and less significantly.



**Fig. 5** Dimensionless fundamental natural frequency versus core-to-face ratio  $h_c/h_l$  ( $\vartheta_0 = 0.5, L = 10h_l, K_w = 10^8, K_p = 10^6$ ): **a** C-C, **b** C-H, **c** H-H

Figure 4 gives the dimensionless fundamental natural frequency versus foam coefficient for different boundary conditions and foam distributions. It is seen that different foam distributions show different variation tendency with foam coefficient. With the increase in foam coefficient, the natural frequency of the foam-I beam keeps rising while that of the foam-II beam keeps falling. As for the foam-III beam, the natural frequency changes slightly with the foam coefficient.

Figure 5 shows the dimensionless fundamental natural frequency versus core-to-face ratio  $h_c/h_l$  for various foam distributions and boundary conditions. It can be seen that the natural frequency increases initially and then decreases with the core-to-face ratio for various boundary conditions. In addition, the frequency difference of MFCS beams with different foam distributions becomes more and more obvious with the increase in core-to-face ratio. This indicates that foam distribution will play more important effect on vibration characteristics of MFCS beams when the core-to-face ratio is high.

### 6 Conclusions

In this paper, the Chebyshev collocation method is applied to study free vibration of sandwich beams with metal foam core. The model is proposed in the framework of the Timoshenko beam theory. Three types of foam distribution are taken into account. The governing equations and boundary conditions are obtained using Hamilton’s principle. The study shows:

- (i) The Chebyshev collocation method has very high rate of convergence and achieves high precision within the range allowed by the effective number of bits of computers for free vibration of MFCS beams.
- (ii) Among different foam distributions, foam-I provides the largest stiffness, while foam-II leads to the smallest stiffness of MFCS beams.

- (iii) With the rise in core-to-face ratio, natural frequencies of MFCS beams increase initially and then decrease, and foam distribution plays more and more important effect on the vibration characteristics.
- (iv) For the foam-I sandwich beam, the natural frequency increases with the foam coefficient. For the foam-II beam, however, the natural frequency decreases with the foam coefficient. As to the foam-III beam, the natural frequency is not sensitive to the foam coefficient.
- (v) The Winkler–Pasternak elastic foundation makes the MFCS beam stiffer and leads to the higher natural frequency.

**Acknowledgements** This research was supported by the National Natural Science Foundation of China (Grant No. 11672071) and the Fundamental Research Funds for the Central Universities (Grant No. N170504023).

### Compliance with ethical standards

**Conflicts of interest** The authors declare that they have no conflict of interest.

### References

1. Smith, B.H., Szyniszewski, S., Hajjar, J.F., Schafer, B.W., Arwade, S.R.: Steel foam for structures: a review of applications, manufacturing and material properties. *J. Constr. Steel Res.* **71**, 1–10 (2012)
2. Chen, D., Yang, J., Kitipornchai, S.: Free and forced vibrations of shear deformable functionally graded porous beams. *Int. J. Mech. Sci.* **108–109**, 14–22 (2016)
3. Jabbari, M., Mojahedin, A., Khorshidvand, A.R., Eslami, M.R.: Buckling analysis of a functionally graded thin circular plate made of saturated porous materials. *J. Eng. Mech.* **140**, 287–295 (2014)
4. Rezaei, A.S., Saidi, A.R.: Application of Carrera Unified Formulation to study the effect of porosity on natural frequencies of thick porous–cellular plates. *Compos. Part B Eng.* **91**, 361–370 (2016)
5. Wang, Y.Q., Liang, C., Zu, J.W.: Examining wave propagation characteristics in metal foam beams: Euler–Bernoulli and Timoshenko models. *J. Braz. Soc. Mech. Sci. Eng.* **40**, 565 (2018)
6. Jasion, P., Magnucka-Blandzi, E., Szyk, W., Magnucki, K.: Global and local buckling of sandwich circular and beam–rectangular plates with metal foam core. *Thin Walled Struct.* **61**, 154–161 (2012)
7. Zheng, Z., Wang, C., Yu, J., Reid, S.R., Harrigan, J.J.: Dynamic stress–strain states for metal foams using a 3D cellular model. *J. Mech. Phys. Solids* **72**, 93–114 (2014)
8. Liu, J., He, S., Zhao, H., Li, G., Wang, M.: Experimental investigation on the dynamic behaviour of metal foam: from yield to densification. *Int. J. Impact Eng.* **114**, 69–77 (2018)
9. Wang, Y.Q., Ye, C., Zu, J.W.: Nonlinear vibration of metal foam cylindrical shells reinforced with graphene platelets. *Aerosp. Sci. Technol.* **85**, 359–370 (2019)
10. Liu, N., Jeffers, A.E.: Isogeometric analysis of laminated composite and functionally graded sandwich plates based on a layerwise displacement theory. *Compos. Struct.* **176**, 143–153 (2017)
11. Liu, N., Jeffers, A.E.: Adaptive isogeometric analysis in structural frames using a layer-based discretization to model spread of plasticity. *Comput. Struct.* **196**, 1–11 (2018)
12. Liu, N., Jeffers, A.E.: A geometrically exact isogeometric Kirchhoff plate: feature-preserving automatic meshing and  $C^1$  rational triangular Bézier spline discretizations. *Int. J. Numer. Methods Eng.* **115**, 395–409 (2018)
13. Hao, Y.X., Chen, L.H., Zhang, W., Lei, J.G.: Nonlinear oscillations, bifurcations and chaos of functionally graded materials plate. *J. Sound Vib.* **312**, 862–892 (2008)
14. Zhang, W., Yang, J., Hao, Y.: Chaotic vibrations of an orthotropic FGM rectangular plate based on third-order shear deformation theory. *Nonlinear Dyn.* **59**, 619–660 (2010)
15. Hao, Y.X., Zhang, W., Yang, J.: Nonlinear oscillation of a cantilever FGM rectangular plate based on third-order plate theory and asymptotic perturbation method. *Compos. Part B Eng.* **42**, 402–413 (2011)
16. Zhang, W., Hao, Y.X., Yang, J.: Nonlinear dynamics of FGM circular cylindrical shell with clamped–clamped edges. *Compos. Struct.* **94**, 1075–1086 (2012)
17. Mao, J.J., Zhang, W.: Linear and nonlinear free and forced vibrations of graphene reinforced piezoelectric composite plate under external voltage excitation. *Compos. Struct.* **203**, 551–565 (2018)
18. Zhang, W., Hao, Y., Guo, X., Chen, L.: Complicated nonlinear responses of a simply supported FGM rectangular plate under combined parametric and external excitations. *Meccanica* **47**, 985–1014 (2012)
19. Guo, X.Y., Zhang, W.: Nonlinear vibrations of a reinforced composite plate with carbon nanotubes. *Compos. Struct.* **135**, 96–108 (2016)
20. Wang, Y.Q., Huang, X.B., Li, J.: Hydroelastic dynamic analysis of axially moving plates in continuous hot-dip galvanizing process. *Int. J. Mech. Sci.* **110**, 201–216 (2016)
21. Ding, H., Chen, L.Q.: Galerkin methods for natural frequencies of high-speed axially moving beams. *J. Sound Vib.* **329**, 3484–3494 (2010)
22. Wang, Y.Q., Zu, J.W.: Nonlinear steady-state responses of longitudinally traveling functionally graded material plates in contact with liquid. *Compos. Struct.* **164**, 130–144 (2017)
23. Qin, Z., Pang, X., Safaei, B., Chu, F.: Free vibration analysis of rotating functionally graded CNT reinforced composite cylindrical shells with arbitrary boundary conditions. *Compos. Struct.* **220**, 847–860 (2019)

24. Wang, Y.Q., Zu, J.W.: Vibration behaviors of functionally graded rectangular plates with porosities and moving in thermal environment. *Aerosp. Sci. Technol.* **69**, 550–562 (2017)
25. Li, C., Miao, B., Tang, Q., Xi, C., Wen, B.: Nonlinear vibrations analysis of rotating drum-disk coupling structure. *J. Sound Vib.* **420**, 35–60 (2018)
26. Wang, Y.Q.: Electro-mechanical vibration analysis of functionally graded piezoelectric porous plates in the translation state. *Acta Astronaut.* **143**, 263–271 (2018)
27. Yang, X.D., Zhang, W., Chen, L.Q.: Transverse vibrations and stability of axially traveling sandwich beam with soft core. *J. Vib. Acoust.* **135**, 051013 (2013)
28. Zhang, W., Chen, J.E., Cao, D.X., Chen, L.H.: Nonlinear dynamic responses of a truss core sandwich plate. *Compos. Struct.* **108**, 367–386 (2014)
29. Hao, W.L., Zhang, W., Yao, M.H.: Multipulse chaotic dynamics of six-dimensional nonautonomous nonlinear system for a honeycomb sandwich plate. *Int. J. Bifurc. Chaos* **24**, 1450138 (2014)
30. Li, X., Yu, K., Zhao, R.: Thermal post-buckling and vibration analysis of a symmetric sandwich beam with clamped and simply supported boundary conditions. *Arch. Appl. Mech.* **88**, 543–561 (2018)
31. Ashby, M.F., Evans, T., Fleck, N.A., Hutchinson, J.W., Wadley, H.N.G., Gibson, L.J.: *Metal Foams: A Design Guide*. Elsevier, Amsterdam (2000)
32. Gibson, L.J.: Mechanical behavior of metallic foams. *Annu. Rev. Mater. Sci.* **30**, 191–227 (2000)
33. Chen, D., Kitipornchai, S., Yang, J.: Nonlinear free vibration of shear deformable sandwich beam with a functionally graded porous core. *Thin Walled Struct.* **107**, 39–48 (2016)
34. Zhang, J., Qin, Q., Xiang, C., Wang, T.J.: Dynamic response of slender multilayer sandwich beams with metal foam cores subjected to low-velocity impact. *Compos. Struct.* **153**, 614–623 (2016)
35. Jing, L., Wang, Z., Ning, J., Zhao, L.: The dynamic response of sandwich beams with open-cell metal foam cores. *Compos. Part B Eng.* **42**, 1–10 (2011)
36. Streck, T., Michalski, J., Jopek, H.: Computational analysis of the mechanical impedance of the sandwich beam with auxetic metal foam core. *Phys. Status Solidi* **256**, 1800423 (2019)
37. Grygorowicz, M., Magnucki, K., Malinowski, M.: Elastic buckling of a sandwich beam with variable mechanical properties of the core. *Thin Walled Struct.* **87**, 127–132 (2015)
38. Yaseer, M., Xiang, C., Gupta, N., Strbik, O.M., Cho, K.: Syntactic foam core metal matrix sandwich composite under bending conditions. *Mater. Des.* **86**, 536–544 (2015)
39. Smyczynski, M.J., Magnucka-blandzi, E.: Thin-walled structures static and dynamic stability of an axially compressed five-layer sandwich beam. *Thin Walled Struct.* **90**, 23–30 (2015)
40. Caliskan, U., Apalak, M.K.: Low velocity bending impact behavior of foam core sandwich beams: experimental. *Compos. Part B* **112**, 158–175 (2017)
41. Winkler, E.: *Die Lehre von Elastizität und Festigkeit*. H. Dörmann, Prague (1867)
42. Akgöz, B., Civalek, Ö.: Bending analysis of FG microbeams resting on Winkler elastic foundation via strain gradient elasticity. *Compos. Struct.* **134**, 294–301 (2015)
43. Mohammadi, K., Mahinzare, M., Rajabpour, A., Ghadiri, M.: Comparison of modeling a conical nanotube resting on the Winkler elastic foundation based on the modified couple stress theory and molecular dynamics simulation. *Eur. Phys. J. Plus* **132**, 115 (2017)
44. Sofiyev, A.H.: Large amplitude vibration of FGM orthotropic cylindrical shells interacting with the nonlinear Winkler elastic foundation. *Compos. Part B Eng.* **98**, 141–150 (2016)
45. Engin Emsen, K.M., Bekir Akgöz, Ö.C.: Modal analysis of tapered beam-column embedded in Winkler elastic. *Int. J. Eng. Appl. Sci.* **7**, 25–35 (2015)
46. Beskou, N.D., Muho, E.V.: Dynamic response of a finite beam resting on a Winkler foundation to a load moving on its surface with variable speed. *Soil Dyn. Earthq. Eng.* **109**, 222–226 (2018)
47. Elishakoff, I., Tonzani, G.M., Marzani, A.: Effect of boundary conditions in three alternative models of Timoshenko–Ehrenfest beams on Winkler elastic foundation. *Acta Mech.* **229**, 1649–1686 (2018)
48. Filonenko-Borodich, M.M.: Some approximate theories of elastic foundation. *Uchenye Zap. Moskovskogo Gos. Univ. Mekhanika, Moscow* **46**, 3–18 (1940)
49. Vlasov, V.Z.: Beams, plates and shells on elastic foundation. *Isr. Progr. Sci. (Trans.)* (1966)
50. Hetényi, M.: A general solution for the bending of beams on an elastic foundation of arbitrary continuity. *J. Appl. Phys.* **21**, 55–58 (1950)
51. Pasternak, P.L.: On a new method of an elastic foundation by means of two foundation constants. *Gos. Izd. Lit. po Stroit. I Arkhitekture, Moscow, USSR* **1**, 1–56 (1954)
52. Zhang, D.P., Lei, Y.J., Adhikari, S.: Flexoelectric effect on vibration responses of piezoelectric nanobeams embedded in viscoelastic medium based on nonlocal elasticity theory. *Acta Mech.* **229**, 2379–2392 (2018)
53. Zhang, H., Ma, J., Ding, H., Chen, L.: Vibration of axially moving beam supported by viscoelastic foundation. *Appl. Math. Mech.* **38**, 161–172 (2017)
54. Sofiyev, A.H., Kuruoglu, N.: Natural frequency of laminated orthotropic shells with different boundary conditions and resting on the Pasternak type elastic foundation. *Compos. Part B Eng.* **42**, 1562–1570 (2011)
55. Şimşek, M., Reddy, J.N.: A unified higher order beam theory for buckling of a functionally graded microbeam embedded in elastic medium using modified couple stress theory. *Compos. Struct.* **101**, 47–58 (2013)
56. Kim, Y.W.: Free vibration analysis of FGM cylindrical shell partially resting on Pasternak elastic foundation with an oblique edge. *Compos. Part B Eng.* **70**, 263–276 (2015)
57. Mechab, B., Mechab, I., Benaissa, S., Ameri, M., Serier, B.: Probabilistic analysis of effect of the porosities in functionally graded material nanoplate resting on Winkler–Pasternak elastic foundations. *Appl. Math. Model.* **40**, 738–749 (2016)
58. Akgöz, B., Civalek, Ö.: A size-dependent beam model for stability of axially loaded carbon nanotubes surrounded by Pasternak elastic foundation. *Compos. Struct.* **176**, 1028–1038 (2017)

59. Froio, D., Rizzi, E., Simões, F.M.F., Costa, A.P.: Universal analytical solution of the steady-state response of an infinite beam on a Pasternak elastic foundation under moving load. *Int. J. Solids Struct.* **132–133**, 245–263 (2018)
60. Coşkun, İ.: The response of a finite beam on a tensionless Pasternak foundation subjected to a harmonic load. *Eur. J. Mech. A/Solids* **22**, 151–161 (2003)
61. Szekrényes, A.: Improved analysis of unidirectional composite delamination specimens. *Mech. Mater.* **39**, 953–974 (2007)
62. Schillinger, D., Evans, J.A., Reali, A., Scott, M.A., Hughes, T.J.R.: Isogeometric collocation: cost comparison with galerkin methods and extension to adaptive hierarchical NURBS discretizations. *Comput. Methods Appl. Mech. Eng.* **267**, 170–232 (2013)
63. Khaneh Masjedi, P., Ovesy, H.R.: Chebyshev collocation method for static intrinsic equations of geometrically exact beams. *Int. J. Solids Struct.* **54**, 183–191 (2015)
64. Yang, J., Chen, D., Kitipornchai, S.: Buckling and free vibration analyses of functionally graded graphene reinforced porous nanocomposite plates based on Chebyshev–Ritz method. *Compos. Struct.* **193**, 281–294 (2018)
65. Magnucki, K., Stasiewicz, P.: Elastic buckling of a porous beam. *J. Theor. Appl. Mech.* **42**, 859–868 (2004)
66. Magnucka-Blandzi, E.: Axi-symmetrical deflection and buckling of circular porous–cellular plate. *Thin Walled Struct.* **46**, 333–337 (2008)
67. Gibson, L.J., Ashby, M.F.: The mechanics of three-dimensional cellular materials. *Proc. R. Soc. A Math. Phys. Eng. Sci.* **382**, 43–59 (1982)
68. Choi, J.B., Lakes, R.S.: Analysis of elastic modulus of conventional foams and of re-entrant foam materials with a negative Poisson’s ratio. *Int. J. Mech. Sci.* **37**, 51–59 (1995)
69. Reddy, J.N.: Microstructure-dependent couple stress theories of functionally graded beams. *J. Mech. Phys. Solids.* **59**, 2382–2399 (2011)
70. Donnell, L.H.: *Beams, Plates and Shells*. McGraw-Hill Companies, New York (1976)
71. Reddy, J.N.: *Energy Principles and Variational Methods in Applied Mechanics*, 2nd edn. Wiley, New York (2002)
72. Trefethen, L.N.: *Spectral Methods in MATLAB*. SIAM, Philadelphia (2000)
73. Wattanasakulpong, N., Chaikittiratana, A.: Flexural vibration of imperfect functionally graded beams based on Timoshenko beam theory: Chebyshev collocation method. *Meccanica* **50**, 1331–1342 (2015)
74. Kitipornchai, S., Chen, D., Yang, J.: Free vibration and elastic buckling of functionally graded porous beams reinforced by graphene platelets. *Mater. Des.* **116**, 656–665 (2017)